

# **Sounding out the river: Seismic and hydroacoustic monitoring of bedload transport in an alluvial river**

Bronwyn Matthews\*<sup>1</sup>, Mark Naylor<sup>1</sup>, Hugh Sinclair<sup>1</sup>, Andrew Black<sup>2</sup>, Richard Williams<sup>3</sup>, Calum Cuthill<sup>1,4</sup>, Matthew Gervais<sup>1</sup>, Michael Dietze<sup>5,6</sup>, Anna Smith<sup>1</sup>

<sup>1</sup>School of GeoSciences, University of Edinburgh

<sup>2</sup>School of Humanities, Social Sciences and Law, University of Dundee

<sup>3</sup>School of Geographical & Earth Sciences, University of Glasgow

<sup>4</sup>School of Engineering, University of Glasgow

<sup>5</sup>Geographical Institute, Georg-August University Göttingen

<sup>6</sup>Geomorphologie, GFZ Potsdam

\*Correspondence to: Bronwyn Matthews, School of Geosciences, University of Edinburgh, Edinburgh EH8 9XP, UK. E-mail: Bronwyn.Matthews@ed.ac.uk

## **Acknowledgements**

We would like to thank the Glenfeshie Estate and Wildland Scotland for their support to the project through access to the field site. Naylor, Sinclair, Black, Cuthill, Gervais and Williams were funded on this project using the NERC Funded Project "Sounding out the River: Monitoring the mobilisation and transport of bedload in mountain rivers" as part of the NERC Digital Environment Program with Grant number NE/T005920/1. Matthews is funded by an EPSRC studentship (EPSRC EP/T517884/1). Smith contributed to the project through their undergraduate research project. For the purpose of open access, the author has applied a Creative Commons Attribution (CC BY) licence to any Author Accepted Manuscript version arising from this submission.

## **Author contributions**

Matthews is the PhD student working on this project who has led the writing of this paper, done the data analysis and produced the figures. Undergraduate student Smith undertook initial analysis of the hydrophone data which informed our field deployment and classification using hydrophones. Naylor designed the field experiment, led the project and co-wrote the paper. Sinclair contributed geomorphological expertise, co-wrote the paper and co-supervised Matthews. Black and Williams provided expertise and experience in monitoring this catchment. Black also contributed wider meteorological and stream gauge data and both Black and Williams were involved in discussing results and editing the manuscript. Technology development that enabled the data to be collected was led by Cuthill and Gervais. Dietze provided expertise in the use of the seismic sensors for environmental monitoring and provided comments on the manuscript.

## **Data availability**

Snippets of the hydroacoustic data are available as supplemental material and all other data is available upon request to the authors.

## **Pre-print statement**

This paper is a non-peer reviewed preprint submitted to EarthArXiv and is in Earth Surface Processes and Landforms (ESPL) revision process.

## **Conflict of interest disclosure**

The authors have no conflict of interest in the materials or subject matter described in the manuscript.

1 Sounding out the river: Seismic and hydroacoustic monitoring of  
2 bedload transport in an alluvial river

3  
4 December 5, 2023

5 **Abstract**

6 Seismological observations provide a non-invasive and continuous means of indirect measure-  
7 ment of fluvial bedload transport (i.e. the transport of coarse granular material as a function  
8 of water depth in rivers). A significant challenge remains in independently characterising the  
9 seismic signature of bedload transport from other sources such as turbulence. Previous research  
10 suggested using the hysteresis relationship between water level and frequency-filtered seismic  
11 power spectrum as a diagnostic tool for identifying bedload transport. We present a unique  
12 dataset from an alluvial Scottish river, including seismic and hydroacoustic measurements, to  
13 analyse bedload transport during three successive high flow events within a year. Examining  
14 data from successive events enabled us to evaluate the consistency of bedload transport thresh-  
15 olds and the influence of past transport events. Our findings reveal that bedload transport was  
16 observed in all three events, with the threshold for entrainment influenced by antecedent events.  
17 Following the largest of the three events the threshold water level for entrainment dropped by  
18 20%, meaning it was easier to mobilise sediment in the subsequent event. We also found that  
19 while hysteresis was observed in the seismic data for the largest event, it was not recorded in the  
20 two other events despite known bedload transport; this implies that a seismic record of hysteresis  
21 alone is insufficient for identifying bedload transport. Our work suggests that there is a greater  
22 richness in the seismic data than has previously been identified and exploited, providing crucial  
23 information for effective river and land-use management in a changing climate with potentially  
24 impacted high flow events.

25 **Keywords**— river, bedload transport, entrainment threshold, fluvial geomorphology, environmental  
26 seismology

# 27 1 Introduction

28 The interplay of climate change and intensified flooding events pose significant threats to both infrastructure  
29 and ecosystems in many areas across the world. Climate change has brought about an increased frequency  
30 and severity of floods in some climates, including in the UK, leading to increased transportation of sediments  
31 and debris by rivers. The transport of coarse gravelly bedload can have significant impacts on infrastructure  
32 such as bridges and dams, and profound ecological consequences, altering riverbed morphology, disturbing  
33 aquatic habitats and negatively impacting aquatic species (Church, 2006; Turowski et al., 2011; Roth et al.,  
34 2017). Additionally, anthropogenic activities, including urban development, deforestation, channelisation of  
35 rivers for river management, as well as re-naturalisation of rivers, alters the patterns of bedload transport  
36 in rivers (Cox et al., 2021). Therefore, being able to monitor and understand the timing and nature of  
37 coarse sediment mobilisation is important for predicting changes in channel morphology and is crucial for a  
38 range of applications, such as ensuring the robust design and maintenance of infrastructure against fluvial  
39 erosion, aiding in effective flood management and response, optimising sustainable use of water resources,  
40 and preserving the health of aquatic ecosystems.

41 The dynamic nature of sediment movement in river systems makes monitoring and measuring the trans-  
42 port of coarse bedload challenging, particularly as rivers erode, aggrade and shift their course. One of the  
43 key challenges lies in accurately measuring the onset of entrainment of bedload in the water column, and the  
44 mobilisation of larger-scale bedforms such as braid bars. Variations in entrainment thresholds are determined  
45 by metrics such as particle shape and size distribution (P. R. Wilcock et al., 2003; Jain et al., 2021), bed-  
46 forms (Church et al., 1998), sediment cohesion (Kothyari et al., 2008), and changes in grain size between the  
47 bed surface and subsurface where coarse sediment may act to armour the river bed (Lisle et al., 1992; Jain  
48 et al., 2021). Using flume tank experiments it has been demonstrated that variations in these characteristics  
49 respond to durations and frequencies of moderate to peak discharge conditions (Ockelford et al., 2019; Luo  
50 et al., 2023). The grain-size distribution may be modified at the bed surface by winnowing of finer grains  
51 resulting in the formation of an armoured surface layer of coarser grains (Pitlick et al., 2009; Gomez et al.,  
52 2022). This armouring modifies the onset of bedload entrainment complicating the relationship between the  
53 measured grain-size distribution and the entrainment threshold. A further complication to the measurement  
54 of bedload transport are hysteresis patterns, where sediment transport rates do not have a linear scaling  
55 with the flow conditions (Bogen, 1980). Armouring is an example of a process that could result in hysteresis  
56 in bedload transport as it may increase the threshold for sediment motion on the bed causing the rising  
57 and falling limbs of a flood hydrograph to have different threshold entrainment values. The mobilisation  
58 of coarse bedload can also be influenced by the suspended sediment concentration at the sediment water  
59 interface (Rickenmann, 1991; An et al., 2018). Suspended sediment loads are commonly higher during the

60 rising limb of flood hydrographs that also results in different entrainment thresholds on either side of a flood.  
61 Such non-linear and thresholded behaviour makes it difficult to predict the timings and intensity of bedload  
62 transport. Temporal variations in the bedload transport thresholds in response to changes in near surface  
63 sediment characteristics have not been documented in alluvial rivers.

64 Addressing these challenges requires innovative site and reach-scale measurement techniques, geomorpho-  
65 logical and hydrological field observations, and sediment transport modelling to gain a more comprehensive  
66 understanding of bedload transport dynamics, and the interplay between sediments, flow dynamics, and  
67 riverbed characteristics. However, since coarse bedload is mobilised when rivers are at high flow, logistical  
68 challenges are introduced when using many measurement techniques. Traditional methods of monitoring  
69 bedload transport in rivers, such as sediment sampling, sediment traps, grain size analysis and flow measure-  
70 ments, have typically relied on direct field measurements and observations. However, these approaches come  
71 with several limitations: sediment sampling and flow measurements can be labour-intensive, time-consuming,  
72 and difficult at high flows, while sediment traps (although continuous in measurement) are prone to errors  
73 due to bedload particles bouncing over or around the traps, and are subject to damage during high flows  
74 (Brasington et al., 2003; Bunte et al., 2004; Bunte et al., 2005; Thorne, 2014). These traditional methods  
75 struggle to capture the full complexity and natural dynamics of bedload transport, as they are typically per-  
76 formed during mild hydrologic events, over short timescales, and during daylight hours. They also generally  
77 only measure at a single point in space, while bedload transport occurs along cross-sections with potentially  
78 variable transport at individual points in space. As a result, they may not provide sufficiently representative  
79 data needed for effective river management, infrastructure design, or understanding sediment transport pat-  
80 terns. Engineers often use numerical models or empirical equations as alternatives to traditional methods  
81 for predicting bedload transport (Geay et al., 2020). However, simplification of these empirical equations  
82 relative to complexities of natural bedload transport processes in rivers, and the challenge of estimating grain  
83 size distribution, entrainment thresholds, and bed morphology among other factors, results in considerable  
84 uncertainties in the sediment transport predictions (Dey, 2014; Downs et al., 2016).

85 Modern technologies and advanced measurement techniques are increasingly being employed to address  
86 these limitations and provide more precise insights into bedload transport dynamics. Several recent studies  
87 have explored the potential for seismic sensors (such as geophones) to be used to monitor environmental  
88 and geomorphic processes (e.g. Burtin et al., 2008; Roth et al., 2016; Dietze et al., 2019a; Lagarde et al.,  
89 2021). Geophones, which are typically used for seismic studies, have important applications in the field of  
90 bedload transport monitoring. Previously, geophones have been strategically deployed in riverbeds or on  
91 river banks to capture the ground vibrations caused by bedload particles interacting with the river bed.  
92 These vibrations can be analysed to estimate the timings, intensity and frequency of bedload transport in

93 rivers. This innovative use of geophones provides a non-intrusive and continuous monitoring method that  
94 overcomes some limitations associated with traditional bedload measurement techniques, facilitating the  
95 monitoring of bedload transport under conditions that were previously not possible (Burtin et al., 2010).  
96 Geophones record a range of environmental signals that are filtered by their passage through the earth. The  
97 potential sources for these signals include precipitation, wind, tides, traffic, turbulent motion in rivers, and  
98 the impact of bedload on riverbeds (W. S. D. Wilcock et al., 1999; Burtin et al., 2008; Rindraharisaona  
99 et al., 2022). Previous studies have focused on the frequency characteristics of seismic energy to discriminate  
100 different sources of seismic noise (Burtin et al., 2008; Burtin et al., 2014; Gimbert et al., 2014). The key  
101 discrimination for river induced seismic signals is between coarse bedload transport and water turbulence.  
102 It has been suggested that bedload transport induces broadband higher frequency seismic waves than the  
103 continuous signal from river turbulence (Schmandt et al., 2013; Gimbert et al., 2014; Vore et al., 2019).

104 By correlating the bedload induced seismic data with river discharge, crucial insights have been gained  
105 into the dynamics of sediment transport and how it responds to variations in hydraulic characteristics. Many  
106 studies found a hysteretic relationship between these parameters which has been interpreted to be evidence  
107 of bedload transport, as significant hysteresis is not expected in the relationship between river stage and  
108 turbulence (Hsu et al., 2011; Turowski et al., 2013; Roth et al., 2016; Roth et al., 2017). As outlined  
109 above, factors like particle size, shape and bed structure can influence the initiation of bedload transport on  
110 rivers, such that sediment entrainment thresholds may vary relative to changes in flow conditions. Bedload  
111 transport may even continue after the water level has begun to decrease, or may initiate and cease at different  
112 levels, since it takes time for particles to be entrained or re-deposited based on the local hydraulic conditions.  
113 This interpretation of hysteresis has become a foundational assumption for many fluvial seismic studies, with  
114 some studies reporting a clockwise pattern of hysteresis where bedload transport peaks before the peak in  
115 water level, and some recording an anticlockwise pattern where the peak in water level occurs prior to the  
116 peak in bedload transport. Clockwise patterns are associated with readily available sediments (Reid et al.,  
117 1985; Kuhnle, 1992; Hassan et al., 2006; Gaeuman, 2010; Mao, 2012; Mao et al., 2014), while anticlockwise  
118 patterns are thought to be caused by processes that increase sediment supply after a flood peak (Reid et al.,  
119 1985; Kuhnle, 1992; Lee et al., 2004; Mao et al., 2014). These previous studies have shed light on the  
120 invaluable use of geophones for bedload monitoring purposes, however they generally had little independent  
121 data to constrain when bedload was being transported.

122 In order to test some of these assumptions used in interpreting geophone data, we combine geophones  
123 with hydrophones to independently classify when coarse bedload is transported. Hydrophones are typically  
124 used to detect and record underwater sound, making them particularly useful for applications in the fields  
125 of marine biology, underwater communication, and sonar systems (Ballance et al., 2023; Bountourakis et al.,

126 2023). In contrast to geophones, hydrophones can record all particle collisions within the local river channel  
127 – collisions between particles and the bed, as well as inter-particle collisions. However, it is more logistically  
128 difficult to deploy them routinely as they have to be placed within a river water column for the duration  
129 of the measurements, thus requiring careful methodological approach and appropriate housing to protect  
130 the instrument during high flow events. On an event-by-event basis they can provide independent data to  
131 critique the seismic bedload transport information obtained from geophones and to test whether hysteresis in  
132 the relationship between the fluvial seismic signal and water level is in fact a fingerprint of bedload transport.

133 Here, we use co-located hydrophones to test the application of geophones in characterising the onset of  
134 coarse bedload transport, and the presence of hysteresis during the passage of a flood hydrograph. Our study  
135 determines bedload mobilisation thresholds and evaluates the influence of antecedent events through inde-  
136 pendent seismic and hydroacoustic characterisations. By integrating seismic, water level, and hydroacoustic  
137 data we aim to gain insights into bedload transport thresholds, examine hysteresis patterns, and shed light  
138 on the intricate relationship between flowing water and sediment. Our analysis focuses on a relatively stable  
139 section of the gravel-bed River Feshie, in the Scottish Cairngorms (Figure 1) and analyses seismic signals  
140 from the three largest flow events in 2022. This enables the consistency of bedload transport entrainment  
141 thresholds to be examined and explored, and the effects of antecedent events on the thresholds observed. Our  
142 findings will contribute to more informed decision-making in river systems management and environmental  
143 protection, by constraining entrainment thresholds and hence enabling calculations and model predictions  
144 of sediment mobility in the channels.

## 145 **2 Methods**

### 146 **2.1 Field site: River Feshie**

147 The River Feshie, in Scotland, is an alluvial tributary of the River Spey and drains a catchment of  $\sim 240\text{km}^2$   
148 with maximum elevation of just over 1200 m (Figure 1) (Ferguson et al., 1983). The bedrock has low  
149 permeability which results in a hydrograph that is very responsive to rain and snowmelt events (Chelmicki  
150 et al., 1999). The headwaters sit on the peat-rich plateau of the Cairngorms (upstream of SG1 in Figure 1)  
151 and then flow downstream through glacial outwash gravels (downstream of SG1 in Figure 1). The Feshie is  
152 supplied largely by the erosion of glacial moraine and outwash channels resulting in a broad, braided gravel-  
153 dominated river (Ferguson et al., 1983; Brasington et al., 2000). We focus on a  $\sim 500\text{m}$  long, single-thread  
154 reach just downstream of a wide multi-thread braided section (Figure 1 and 2). Within the study site, the  
155 channel width varies between 25 m to 70 m and has a local slope of  $\sim 0.006$ . The bedrock is predominantly  
156 Moinian schist and granite which dominate the bedload. The average grain sizes in the bar adjacent to the

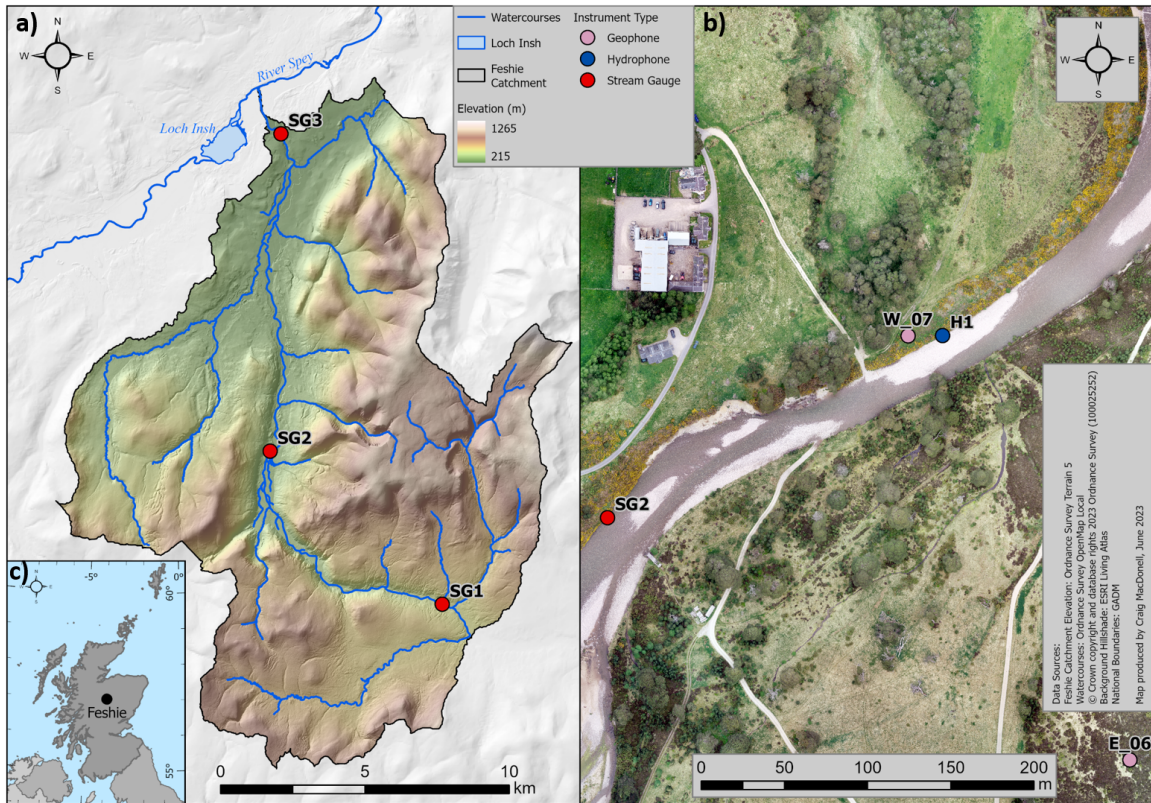


**Figure 1:** Maps of the River Feshie fieldsite at the (a) catchment scale showing the three stream gauge sites, (b) reach scale showing the sites of instruments used in this study, and (c) national scale. Photos of the field deployments can be found in Supplemental Material S1.

157 geophone station measured using the Wolman pebble count method (Wolman, 1954) routinely before and  
 158 after the 2022 events are:  $D_{16} = 14$  mm,  $D_{50} = 35$  mm and  $D_{84} = 72$  mm.

159 In the late 1970s a stream gauge was maintained in the same stretch as our study site by Ferguson et al.  
 160 (1983) and recorded a mean flow of  $3\text{--}4$   $\text{m}^3\text{s}^{-1}$  with regular floods reaching  $20\text{--}30$   $\text{m}^3\text{s}^{-1}$  and the largest floods  
 161 recorded exceeded  $100$   $\text{m}^3\text{s}^{-1}$ . A stream gauge that is currently located approximately 12 km downstream  
 162 at Feshiebridge (SG3 in Figure 1), maintained by SEPA (Scottish Environment Protection Agency), reveals  
 163 the same variable flow regime with peak flows exceeding  $100$   $\text{m}^3\text{s}^{-1}$  and a maximum peak flow of  $260$   $\text{m}^3\text{s}^{-1}$ .  
 164 From flow data over the last 7 years at Feshiebridge (SG3) (Figure 3) it can be seen that there are generally  
 165 larger flows occurring during winter and spring. Flow patterns of 2022 were generally similar to previous  
 166 years with low flows during summer and larger peaked flows in spring, autumn and winter. Summer flows in  
 167 2022 were particularly low, and were bounded by large events in early spring and autumn. The largest event  
 168 of 2022, which we use for this analysis, peaked at around  $138$   $\text{m}^3\text{s}^{-1}$ . Prior to this there had only been six  
 169 other peaks that exceeded this level over the 7 years (Figure 3); the largest of these occurring in December  
 170 2015 as a result of Storm Frank that caused widespread flooding across much of Scotland, Northern England

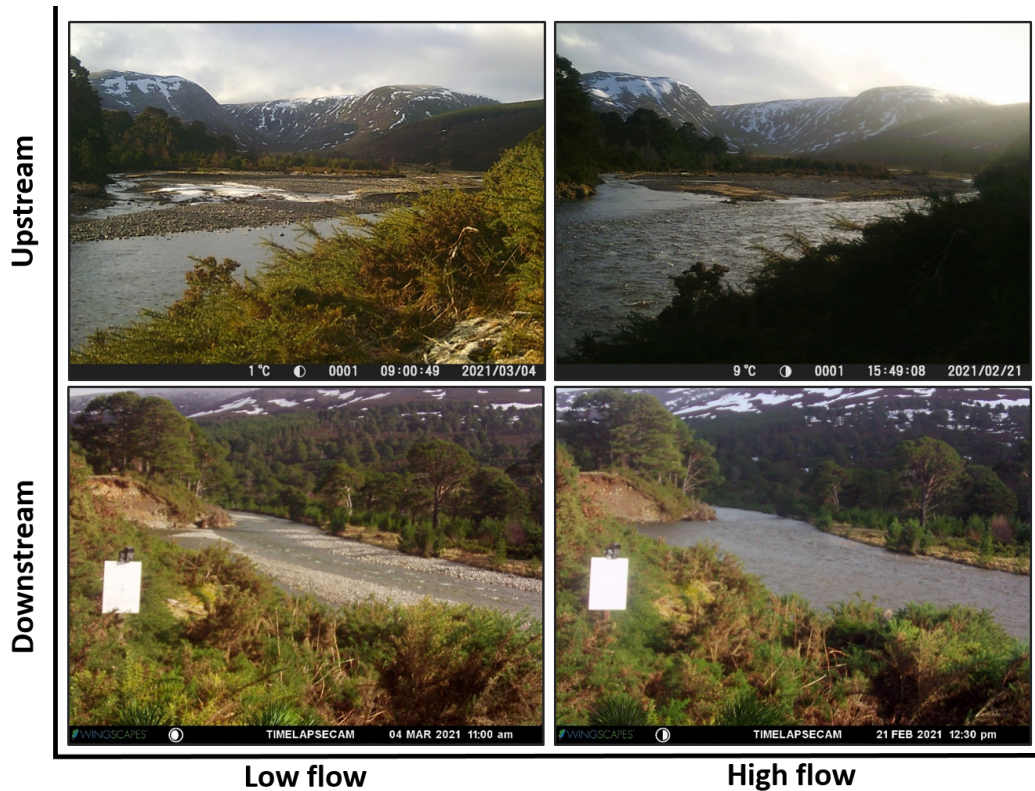


**Figure 2:** Photos from the River Feshie fieldsite looking upstream and downstream from SG2 during high flow and low flows. Images are taken from February and March 2021 as these had the clearest conditions and are representative of general high and low flows at the site. During the low flow event the SEPA stream gauge at SG3 measured a water level of 0.76 m and the high flow event photographed here peaked at 2.15 m at SG3.

171 and Wales (Barker et al., 2016).

## 172 2.2 Data collection

### 173 2.2.1 Stream Gauge Data

174 This study uses water level (stage) measurements recorded at three stream gauge sites on the River Feshie.  
 175 To measure water level at our study site, we deployed a LiDAR (Light Detection and Ranging) water level  
 176 sensor on the remains of a footbridge at site SG2 which takes repeat measurements of the distance to the  
 177 water surface every 5 minutes. Using this data combined with channel geometry measurements, we have  
 178 been able to convert to discharge values, however we will be using stage data in this analysis as it is more  
 179 accurate measured data. We also have access to water level and discharge data collected every 15 minutes  
 180 at stream gauges SG1 and SG3, located approximately 10km upstream and downstream of our site (Figure  
 181 1). These data are managed by Dr Andrew Black (University of Dundee) and SEPA, respectively. We use  
 182 the SEPA data as the historic record since our local sensor has only been operational since the end of 2020.



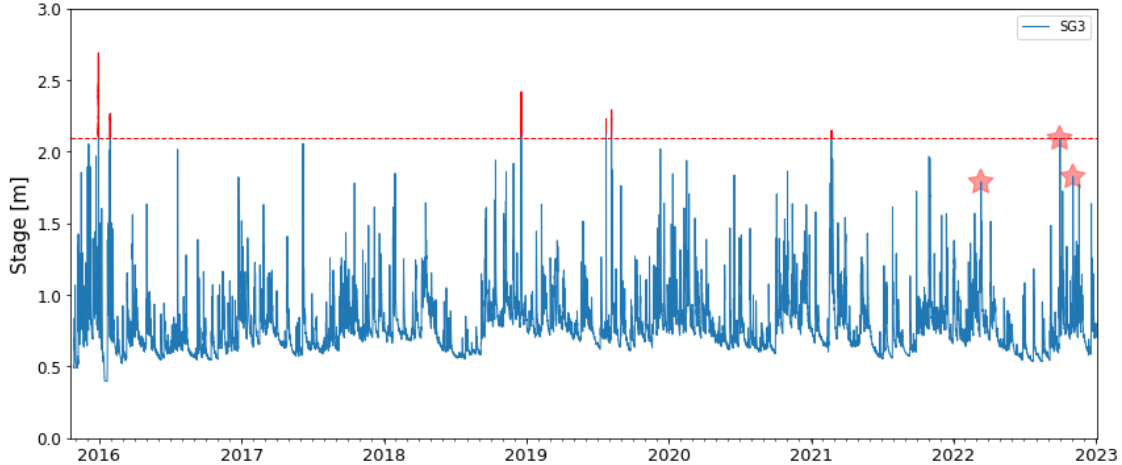


**Figure 3:** Stage measurements from SEPA stream gauge at SG3 from 27th October 2015 to 31st December 2022. Red stars mark the three largest events in 2022 that are analysed in this study. Red line marks the water level of the largest event in 2022, with peaks that have previously exceeded this value also marked in red.

183 The three events analysed in this study occurred on the 11<sup>th</sup> - 14<sup>th</sup> March 2022 (three successive peaks  
 184 with a maximum water level of 1.27 m at SG2), 30<sup>th</sup> September - 1<sup>st</sup> October 2022 (one peak with a  
 185 maximum water level of 1.69 m at SG2, a roughly once-in-a-year event), and 2<sup>nd</sup> - 3<sup>rd</sup> November 2022 (one  
 186 peak with a maximum water level of 1.30 m at SG2). These events are herein referred to as the ‘March  
 187 event’, the ‘September-October event’, and the ‘November event’, respectively. The March event follows a  
 188 series of snowmelt cycles that caused three repeated peaks in water level, resulting from rainfall on snow  
 189 combined with snowmelt and reaches a peak discharge of  $84 \text{ m}^3\text{s}^{-1}$  at the SEPA station SG3. The larger  
 190 September-October event is of a shorter duration and occurs following intense precipitation in the catchment  
 191 that coincides with the tailend of Hurricane Fiona that hit Canada in mid-late September 2022, resulting in  
 192 peak discharge of  $131 \text{ m}^3\text{s}^{-1}$  at SG3. The November event is an early winter storm with similar magnitude  
 193 to the March event, however it occurs as a result of high rainfall alone, reaching peak discharge at  $90 \text{ m}^3\text{s}^{-1}$ .  
 194 The three peaks in the first event allow us to test the consistency of the onset of bedload, the second event  
 195 allows us to explore the impact of a large event on these thresholds of motion, and the final event allows  
 196 us to explore the new behaviour of the river after a large event. Thus combining data from successive high  
 197 flow events demonstrates how the technique can be used to make inferences about the effects of antecedent  
 198 events on the mobilisation of bedload.

### 199 **2.2.2 Seismic and Hydroacoustic Data**

200 This study integrates seismic and hydroacoustic data to study the mobilisation and transport of bedload  
 201 along a short ( $\sim 100 \text{ m}$ ) stretch of the River Feshie (Figure 1). We use the co-located stream gauge sensor

202 (SG2) to analyse the water level dependence of the seismic and hydroacoustic data.

203 We compare data from two 3-component PE6B (4.5Hz) geophones connected to Digos DataCube loggers  
204 recording at a sampling rate of 200 Hz. The geophone data is continuously recorded. The geophones are  
205 buried in soil at approximately 10 cm depth (base of instrument to surface), levelled and oriented with the  
206 North-South (horizontal) component aligned along the downstream river direction. The geophone at site  
207 W\_07 is located within approximately 5 m of the river and 1 m above the base level water surface. It is well  
208 sited to record a strong river signal as the small source-to-sensor distance minimises the attenuation of high  
209 frequencies, which is important for this study as we are wanting to resolve frequencies of bedload transport  
210 (Figure 1). The other geophone at site E\_06 is located approximately 300m from the river as a control  
211 site to characterise other sources of environmental noise, such as precipitation and wind as the impact of  
212 rain on the ground and the movement of vegetation by wind can be recorded by geophones (Dean, 2018;  
213 Rindraharisaona et al., 2022). Both sites have similar geology with high-velocity Moinian schist bedrock  
214 overlain by low-velocity glacial till. Signals which are common to both W\_07 and E\_06 we identify as non-  
215 river environmental noise, and this approach allows us to confirm that the relatively high broadband noise  
216 level prior to the water rising is due to hydrometeorological noise. Generally, seismic bedload studies have  
217 used the vertical component of seismic waves as, due to the impact direction of bedload on the river bed, it  
218 was assumed that the emitted seismic waves would be best represented by Rayleigh waves with strong vertical  
219 displacements (Tsai et al., 2012; Dietze et al., 2019b). Here, we present the analysis of the stream-parallel  
220 component. This was chosen because, although using the vertical and the stream-perpendicular components  
221 for the analysis gave similar results, the vertical component tended to be noisier due to its susceptibility  
222 to rain interference (see Supplemental Material S2) and theoretically the stream-parallel component should  
223 give the strongest river-related signal (Roth et al., 2016). The area is anthropogenically very quiet with  
224 little traffic on the estate roads, and so there is minimal interference from these sources. The geophones  
225 are expected to record both the interaction of turbulence in the water with the bed and direct collisions  
226 of particles with the bed. It has previously been found that seismic waves emitted from bedload collisions  
227 resulted in higher frequencies than those from turbulence, with bedload generally found to occur in the range  
228 of 30-60 Hz and turbulence around 1-20 Hz (Tsai et al., 2012; Gimbert et al., 2014; Dietze et al., 2019a).

229 To independently characterise the bedload motion recorded within the study site, we deployed a hy-  
230 drophone (Jez Riley French D-series) within the river at site H1 connected to our own Raspberry Pi logger,  
231 to record the hydroacoustic signal of turbulence and bedload motion. In previous hydroacoustic studies  
232 hydrophones have been deployed in metal pipes or attached to metal plates embedded in the river bed  
233 (Barrière et al., 2015), attached to the bottom of boats or river surveying equipment such as river boards  
234 (Geay et al., 2020), or attached to man-made infrastructure, such as bridges or metal frames (Belleudy et al.,

235 2010), however this was logistically not an option in our study site. Instead, the hydrophone was mounted  
236 within a roughly 40 kg (0.4 m x 0.3 m x 0.3 m) granite block with a hollow cylindrical core of diameter 0.2  
237 m in order to protect it from damage by direct impacts from mobile material (see Supplemental Material  
238 S1). The hydrophone block is located approximately 5 m downstream of the geophone at site W\_07 and  
239 40cm from the river bank (Figure 1). The recording system is built using a PiZero, a Witty Pi for scheduling  
240 and a HiFiBerry DAC+ADC Pro sound card (sampling at 44.1 kHz); due to the size of the datafiles, we  
241 record a 30 second sample every 15 minutes. Data are recorded at two different gains of 30 dB and 40 dB to  
242 manage potential issues of data quality. In addition to measuring collisions between particles and the bed,  
243 like geophones, hydrophones also record collisions of particles in suspension. The hydroacoustic data is used  
244 as a complementary data set to the seismic data to confirm the occurrence and timing of bedload motion.

### 245 **2.3 Data processing and analysis**

246 We preprocess the seismic data by removing the instrument response through ObsPy using information  
247 provided by Digos on the specific instrument used. We then apply a bandpass filter in the frequency domain  
248 (between 4.5 Hz and 99 Hz) to the data prior to deconvolution to remove the frequencies most affected by  
249 the instrument itself. The data is then detrended to remove the mean trend of the signal using ObsPy. We  
250 computed the power spectral density (PSD) using Welch’s method (Welch, 1967) with a 1-minute window  
251 and no overlap, to quantify the variation in seismic power as a function of time and frequency, which we  
252 compare to water level. In order to isolate the bedload signal, the standard methodology is to then average  
253 the PSD over the relevant frequency bands (Tsai et al., 2012; Bakker et al., 2020; Lagarde et al., 2021).  
254 This frequency range is typically around 30-60 Hz with turbulence found to be approximately 1-20 Hz (Tsai  
255 et al., 2012; Gimbert et al., 2014; Dietze et al., 2019a). This approach allows us to compute the PSD for the  
256 seismic energy recorded within the frequency range commonly associated with the appearance of bedload  
257 transport. The data is plotted as a visual representation of the frequencies of the signal over time as a  
258 spectrogram and then as a time varying PSD plot to show the temporal change in seismic power over the  
259 chosen frequency bands.

260 The raw hydroacoustic data contains a lot of information about the processes occurring in the river.  
261 There is a distinct audible signal from turbulence (gurgling), smaller grain sizes being transported (tinkling  
262 and tapping), and larger grain sizes being transported (thudding and knocking), which can be used to  
263 manually classify the dominant process (see Audio 1-3). For the duration of each of the three high flow events  
264 considered here, the 30 second hydroacoustic recordings taken every 15 minutes were manually categorised by  
265 whether bedload was being transported and whether it was not. The recordings were categorised as ‘Bedload  
266 Transport’ if they were dominated by moving pebbles with more than 10 pebble hits over a 5 second window,

267 however if there was only the occasional pebble movement (<10 per 5 seconds) and it was dominated by  
268 turbulence noises the files were classified as 'No Bedload Transport'. The categorisation into the larger and  
269 smaller grains being transported is a bit more ambiguous as it relied on an audible identification of a change  
270 in frequency, and more work could be done to look at the frequency characteristics of the hydroacoustic data.  
271 The same researcher processed all the hydroacoustic data to minimise errors in the categorisation. At low  
272 water levels ( $\sim 0.6$  m) the hydrophones are exposed and therefore don't record any river related signals so  
273 are excluded from our analysis. Categorising the hydroacoustic data provides independent evidence of when  
274 bedload is being transported that we can overlay on the seismic analysis to test the thresholds of entrainment  
275 for coarse bedload and whether bedload transport and hysteresis in the PSD are directly related.

276 The water level data collected on-site was corrected for the height of the sensor above the riverbed to  
277 provide approximate water depth measurements, assuming the river bed was fixed. All stream gauge data,  
278 including that accessed from gauges SG1 and SG3, were linearly interpolated and resampled to one-minute  
279 intervals so that they could be combined with the geophone data that was analysed in minute long windows.  
280 Since the water level hydrographs during a high flow event are fairly smooth it is easy to interpolate between  
281 the 15 minute samples. This also provided us much more richness in the data, as resampling the geophone  
282 data to 15 minute intervals to match the original stream gauge data sample rate would potentially miss  
283 important information from the propagating flood waves.

## 284 **3 Results**

285 The results compare the co-located geophone and hydrophone data at site W\_07 and H1, respectively, and  
286 geophone data collected at a control site approximately 300 m away from the river (E\_06). This comparative  
287 analysis is supported by locally measured stream gauge data from SG2 (Figure 1c). The results discuss  
288 the river-induced seismic signals at the two geophone sites, the observed transport thresholds over three  
289 successive high flow events, and the robustness of using hysteresis as a fingerprint of bedload transport.

### 290 **3.1 Comparison of the river site with the non-fluvial control site**

291 First we compare and contrast the geophone data recorded beside the river (W\_07) and at the control site  
292 (E\_06) in order to discriminate background environmental signals from those sourced from the river channel.

293 The water-level time series and spectrograms derived from the geophone data at each site are plotted in  
294 Figure 4 for two different events. The plots in each column have common time axes; the November event is  
295 not shown because the control site geophone E\_06 was not recording at this time. Prior to the water rising,  
296 all the spectrograms show vertical broadband streaks of high amplitude (approximately -140 to -145 dB),  
297 which correspond to the periods of rain that necessarily precede the water level rising as we observed no

298 snowmelt-only hydrological events (Figure 4 (c-f)). Similarly, when the water level is dropping, it is likely  
 299 that there will be less rain at the site, and fewer vertical streaks on the spectrogram, as the water level  
 300 would not be dropping if there was still significant rain across the catchment. This assumption does not  
 301 necessarily hold true for large catchments as local conditions may vary from catchment wide conditions, such  
 302 as rainfall patterns, however our interpretation makes this assumption due to the relatively small catchment  
 303 size. Some of these streaky broadband signals could also be a result of wind but it is difficult to differentiate  
 304 the two without further meteorological data as they tend to have similar characteristics and occupy similar  
 305 frequency bands (Rindraharisaona et al., 2022).

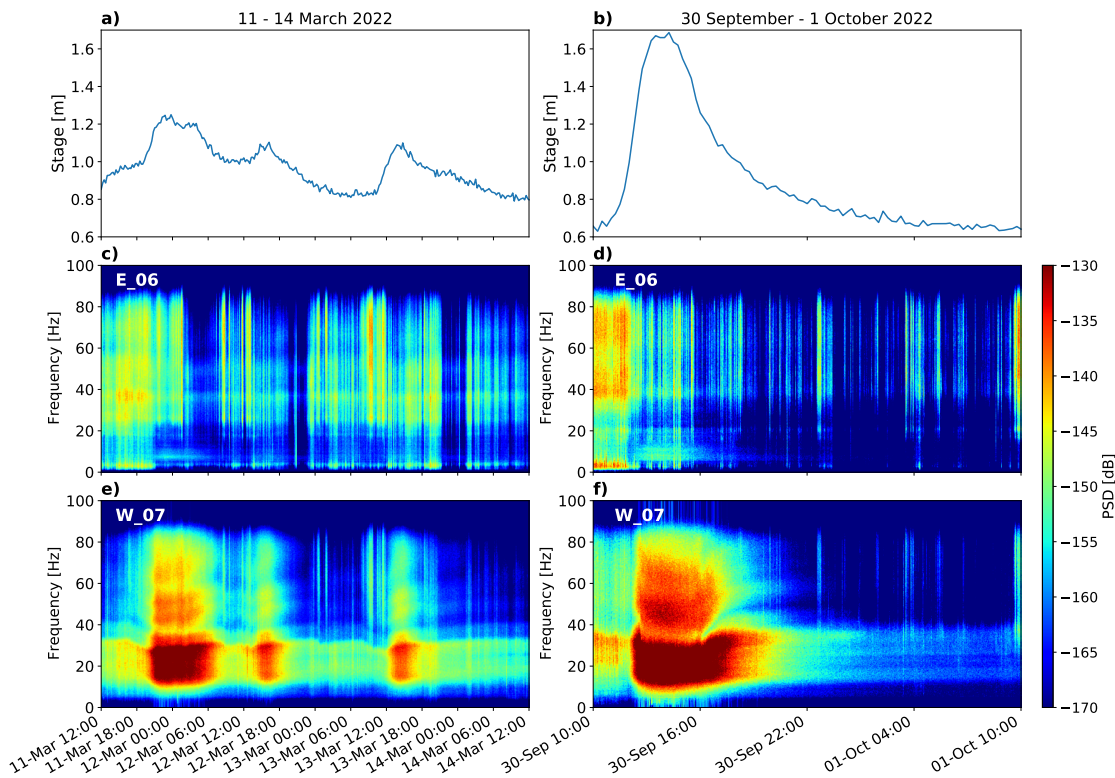


**Figure 4:** Data for two distinct high flow events in March and September-October 2022, one in each column. Included in this plot are; (a, b) the time-series of the water level at SG2, (c, d) the spectrograms of the geophone data (in 1 minute windows) at the control site to highlight environmental noise such as wind and rain, and (e, f) the spectrograms of the geophones at the river site which is dominated by signals of turbulence and sediment transport.

306 In contrast to the control site we see that the PSD time-series measured at the river bank station, W\_07,  
 307 evolves as the water level changes. During periods of base level flow, when the water is low, the greatest  
 308 power is recorded within a frequency range of approximately 5-35 Hz and is continuous, even during low  
 309 flows prior to and following the large events, which suggests this is the background river signal (turbulence);  
 310 this feature is absent at the control site. This value is slightly higher than those found in previous studies  
 311 (as previously discussed in the 2 Section) but is most likely a result of site characteristics. The sudden onset

312 of higher frequency (30-80 Hz) high power seismic signals at W\_07 recorded during the peak of the flood  
313 waves suggests that there is a separate signal in addition to that derived from turbulence. During the highest  
314 water levels, these high power bands extend to higher frequencies, up to around 85 Hz, but once the river  
315 level drops back down towards base levels these higher frequency signals become less dominant. These high  
316 power, high frequency signals are also absent from the control site, thus enforcing the interpretation that  
317 these are river related signals, but the hydroacoustic data will help clarify this. These comparisons allow  
318 us to identify the seismic signals that are induced by river-related processes, and specifically those induced  
319 by bedload transport, which are then used throughout the rest of this study to analyse transport thresholds  
320 and patterns.

## 321 **3.2 Analysis across three successive high flow events**

322 Having documented the fingerprints of different physical processes within the time-frequency domain (Figure  
323 4), we simplify the analysis by focusing on the 30-80 Hz band, as previous studies (e.g. Burtin et al., 2008;  
324 Roth et al., 2016; Turowski et al., 2015) have found that bedload transport produces signals at higher  
325 frequencies than turbulence, which going by our interpretation from Figure 4 would be  $>30$  Hz. Specifically,  
326 in minute long windows shown in the spectrogram, we average the values of the power over the 50 to 60  
327 Hz range for three distinct high flow events to calculate a single scalar value at each time, which we refer  
328 to as the average power spectral density (aPSD) in the coming plots (See Section 2: Data processing and  
329 analysis). This narrower frequency range was chosen as there was less influence from meteorological and  
330 turbulence seismic signals, making the bedload transport the strongest signal observed for those frequencies.

331 The aPSDs calculated using the selected frequency band of 50-60 Hz highlight the use of site E\_06 as  
332 a control site and the strength of the river-induced seismic signals recorded at W\_07. At the control site  
333 the PSD is dominated by the contributions from the broadband intermittent meteorological (wind and rain)  
334 signal. Consequently the aPSD shows a large amount of scatter that is independent of the water level (Figure  
335 5 a,b). In contrast, the aPSD at the site beside the river, W\_07, mirrors the variations in water level for  
336 all three events, showing a close parallel between the two (Figure 5 c-e). The meteorological noise is still  
337 visible at site W\_07 prior to the hydrological peaks, but the river-induced seismic noise is dominant above  
338 base water levels ( $\sim 0.90 - 1.10$  m) as turbulence increases and bedload begins to mobilise.

### 339 **3.2.1 Entrainment thresholds of coarse bedload**

340 Using the hydrophone data, we classify whether bedload is being transported, independently of the geophone  
341 data, and include this information on the water-level versus aPSD plot (salmon and red shaded regions in  
342 Figure 5 c-e, with blue shading for when only turbulence was observed and white regions when the hydrophone

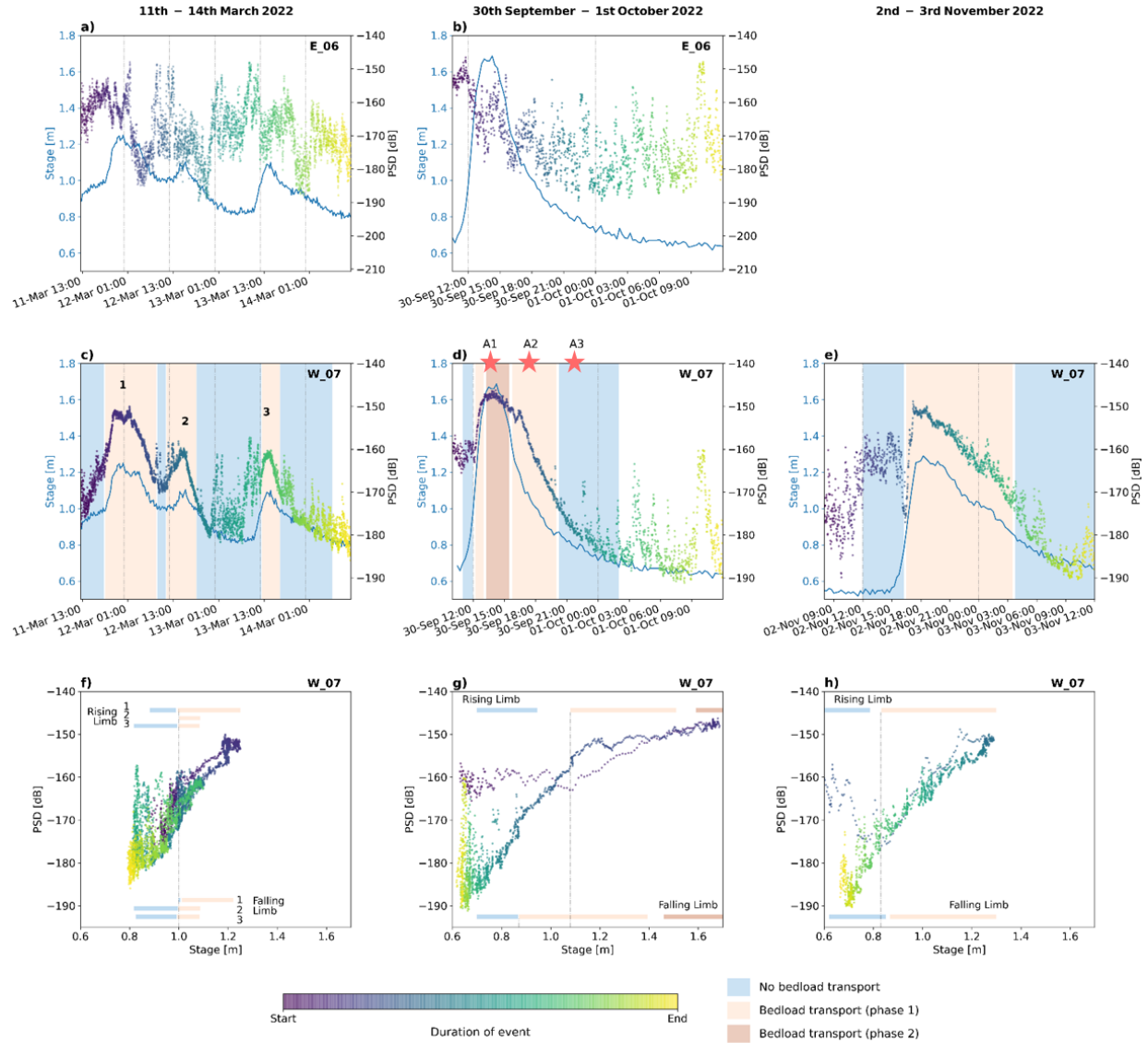


**Figure 5:** Plots summarising the time series of the water level (blue line) and seismic power averaged over the frequency range 50-60 Hz (points coloured by time) for the three largest flow events in 2022. Each column displays a different event showing; (a, b) the aPSD and water level timeseries' for the control site highlighting the environmental noise around the water level peaks, (c, d, e) the aPSD timeseries for the river site layered on top of the independent classification of bedload transport activity using the hydroacoustic data (white shading shows gaps in the data or when the hydrophone was exposed, blue shows periods where the hydrophone records only turbulence, salmon shows when bedload transport starts (phase 1) and red shows when there is an audible shift to lower frequencies on the hydrophone interpreted to be mobilisation of larger grains during bedload transport (phase 2)), (f, g, h) the PSD versus stage relationship with the hydrophone bedload transport classifications shown as bars for the rising and falling limbs of the hydrological peaks. Red stars in d) show the timings of the hydrophone recordings included in Audio 1-3, labelled A1, A2 and A3.

343 was exposed out the water). All three of the high flow events resulted in the mobilisation of bedload during  
 344 the peaks in water level, with the salmon colour, labelled 'Bedload transport (phase 1)' indicating the

345 movement of bedload material. During the largest of the three events (the September-October event) there  
346 was also an audible shift in frequency of the recordings at the highest water level ( $>\sim 1.50 - 1.60$  m), which is  
347 shown in the reddish colour and labelled ‘Bedload transport (phase 2)’ in Figure 5d at the peak of the event,  
348 which lasted approximately 135 minutes. Recordings during the two transport phases and the turbulence  
349 phase (Audio 1-3) highlight the audible changes during these processes. This audible frequency drop in  
350 the hydroacoustic data coincides with a shift to lower frequencies in the geophone data seen in Figure 4f  
351 and Supplemental Material S2, where the lower frequency end of the high amplitude seismic power dips  
352 from about 40 Hz to around 30 Hz at the same time as the peak of the hydrograph and then rises back up  
353 following the peak. The gaps between the hydroacoustic categorisations in Figure 5 c-h are due to the 15  
354 minute hydroacoustic sampling interval resulting in an uncertainty in the water level at which mobilisation  
355 of coarse bedload starts. Here, this water level uncertainty is greater during the rising limb than the falling  
356 limb (Figure 5f-h) due to the rapid rate of increase in water level relative to the quarter-hourly hydrophone  
357 recordings compared to the gradually waning falling limb. Similar features would be observed in a rapidly  
358 decreasing flow, however this was not the case in the events analysed here.

359 Further, we can compare the timing of onset of bedload transport with the water level at that time to  
360 explore any systematic changes in the threshold for motion and arrest across the three events. Figures 5 and  
361 6 reveal that bedload mobilisation during the moderate scale March event consistently starts and stops at a  
362 water level of  $\sim 1.00$  m. This is the case across all three daily peaks, labelled 1-3 in Figures 5c and 6b and c.  
363 However, during the largest September-October event it is observed that coarse bedload transport initiates  
364 at between 0.95 m and 1.08 m, accounting for the uncertainty in the sampling period of the hydroacoustic  
365 data. The previously mentioned audible drop in frequency of the hydroacoustic data occurs between 1.50 m  
366 and 1.59 m and continues throughout the peak (at 1.69 m) and falling limb and stops at around 1.39 - 1.44  
367 m, labelled ‘Bedload transport (phase 2)’ in Figure 5 and 6. At this point on the falling limb the audible  
368 frequency increases to similar to the initial mobilisation and bedload transport is sustained until the water  
369 level drops to  $\sim 0.87$  m. The September-October event therefore had coarse bedload mobilisation initiating  
370 at  $\sim 1.00$  m on the rising limb and ceasing at  $\sim 0.87$  m on the falling limb. The third event in November is  
371 much like the early March event in that the mobilisation of bedload starts and stops at the same level on the  
372 rising and falling limb of the hydrograph. However, for this event the entrainment threshold is now followed  
373 through from the September event at  $\sim 0.79 - 0.87$  m.

### 374 **3.2.2 Hysteresis as a fingerprint of bedload transport**

375 Now consider the water-level versus aPSD plots in Figure 5 f-h and Figure 6a. These allows us to test the  
376 validity of the assumption that hysteresis in the water level versus PSD is a reliable fingerprint of bedload



377 transport. As noted above, bedload transport occurred during all three events which was evidenced through  
378 the hydroacoustic data. Looking at the water level versus aPSD plots it is clear that both the March and  
379 November events have relatively linear relationships and show no signs of hysteresis despite independent  
380 evidence from the hydroacoustic data that bedload was actively being transported. They also show very  
381 similar gradients of aPSD against water level for both the rising and falling limbs, suggesting that the nature  
382 of coarse bedload transport is similar for both events. In contrast, the aPSD analysed over the 50-60 Hz  
383 range in the larger September-October event does exhibit some anticlockwise hysteresis, but only between  $\sim$   
384 1.00 m and 1.40 m. In addition the slope of the aPSD versus water level is lower at higher water levels (Figure  
385 5g). Until around 12:00 on the 30th September (at water levels  $\geq$  1.00 m), the aPSD is relatively constant  
386 at around -160 dB for this event whilst the precipitation dominates the signal, as evidenced in Figure 5 d  
387 and discussed above in section 3: Comparison of the river site with the non-fluvial control site. Once the  
388 water level reaches  $\sim$ 1.00-1.10 m, the aPSD starts to rise at a similar gradient to the other two events but at  
389 slightly lower PSD values (Figure 5f and h; Figure 6). This occurs at a very similar entrainment threshold  
390 to what was observed through the hydroacoustic data, discussed above. At around 1.40 m the aPSD has  
391 risen to approximately -148 dB, and now levels off slightly. One possible cause for a levelling off like this  
392 could be due clipping of the waveforms when the recorded signal exceeds the upper limit of the geophones  
393 recording range, resulting in a loss of data. However, this is not the case here and the observed behaviour  
394 is real (See Supplemental Material S3). This much lower gradient is sustained up to the peak of the event  
395 and continues with the falling limb until  $\sim$ 1.15 m, at which point the gradient returns similar to the original  
396 gradient. This sustained lower gradient lasts longer on the falling limb than the rising limb, which can also  
397 be seen on the aPSD timeseries in Figure 5d where the aPSD remains close to peak levels for a short time  
398 after the peak even once the water level has begun to decrease.

399 In summary, the initial entrainment threshold that was observed in March 2022 dropped by about 15-  
400 20% ( $\sim$ 1.00 m to  $\sim$  0.80-0.85 m) following the September-October event peak and this new lower threshold  
401 was maintained for the subsequent November high flow event. The March and November events show no  
402 hysteresis whereas the larger September-October event shows a degree of anticlockwise hysteresis for water  
403 levels between  $\sim$  1.00 m and 1.40 m (when bedload transport is observed to initiate), and then behaves  
404 linearly at water levels above 1.40 m. Unfortunately, due to the noise from meteorological signals at the  
405 initial stages of the high flow events, it is difficult to identify any features in the seismic data that would  
406 indicate the initial transport of the coarse bedload, which is why the hydroacoustic data has proven very  
407 useful in this analysis.

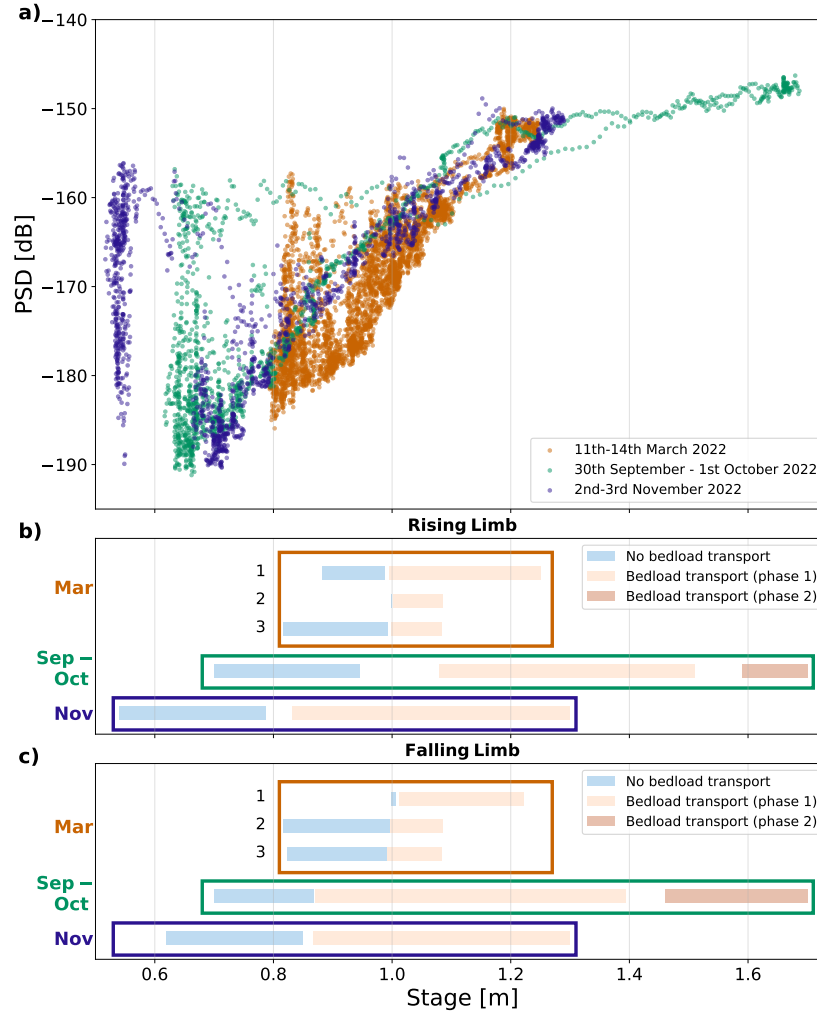


**Figure 6:** (a) Superposition of the PSD versus water level relationships for three distinct high flow events to enable a clearer comparison of the similarities and differences between each event. (b) Bedload activity transitions from independent interpretation of hydroacoustic data that occurred on the rising limbs of flood peaks for all three events; note that for the March and September events bedload started being transported at a water level of  $\sim 1.00$ - $1.10$  m whilst transport during the November event initiated at a water level of  $\sim 0.80$  m. (c) Bedload activity transitions from independent interpretation of hydroacoustic data that occurred on the falling limbs flood peaks for all three events; note that for the March event bedload stopped being transported at a water level of  $\sim 1.00$  m whilst the arrest of bedload transport occurred at  $\sim 0.85$  m for the September and November events.

## 408 4 Discussion

409 From seismic and hydroacoustic measurements at our field site in the alluvial River Feshie, it is clear that  
 410 we can record information on the mobilisation of coarse bedload. One key finding is that the coarse bedload  
 411 transport threshold, and hence bed strength, depends on the recent history of larger discharge events. We  
 412 believe that the largest event observed in 2022 leaves disordered material on the surface of the bed that is  
 413 easier to re-mobilise than it was prior to the large event (Jain et al., 2021). It was observed during routine

414 field visits that the grain size distribution was not sorted before nor after the event. We therefore interpret  
415 the change in entrainment threshold as a consequence of changes in the grain structure and sorting on the  
416 river bed (Jain et al., 2021) with greater deposition of unsorted material; this is consistent with the very  
417 rapid fall in water level inhibiting the bed to find a stable form (Luo et al., 2023). It was also visually  
418 observed that there was no significant change to the width of the channel or the elevation of the bed. The  
419 water depth at which entrainment was initiated changed by  $\sim 15$  cm, but the bed elevation is unlikely to  
420 have changed by this amount, therefore this is unlikely to have had an effect on the thresholds observed. We  
421 hypothesise that, in the absence of a further large flow event like the September-October 2022 event, over  
422 cycles of moderate scale events, such as snow melt cycles or moderate rainfall events like the March and  
423 November events, the bed will progressively regain its strength as the clasts locally reorganise and the water  
424 level threshold for mobility will again rise to a higher value (Ockelford et al., 2019; Luo et al., 2023). This  
425 hypothesis is supported by the observation that in the initial March event, the daily rainfall plus snowmelt  
426 cycles were just sufficient to initiate the motion of bedload at their peak suggesting that these moderate  
427 events have helped the system find a more stable configuration over time. Since events of a similar size to  
428 the March and November events are expected to happen approximately once every 5-6 months, the river will  
429 undergo somewhat frequent local sorting of material before a large approximately one in one year event like  
430 the September-October event breaks through the sorted material and causes large amounts of resorting.

431 Prior to this study, hysteresis in the water-level versus seismic PSD plot was viewed as a digital fingerprint  
432 for bedload transport (Burtin et al., 2008; Hsu et al., 2011; Turowski et al., 2015). In our study bedload was  
433 transported in all three events, but hysteresis in the high frequency signal only occurred in the largest event  
434 when using co-located stream gauge data from SG2; thus using hysteresis alone as an indicator of bedload  
435 transport is insufficient to detect transport events. Our findings are in agreement with Roth et al. (2017)  
436 who found that hysteresis may not be an effective measure of bedload transport as they identified that the  
437 seismic power tracks more closely to the changing water levels than the sediment transport rates measured  
438 using impact plate geophones. In our field site, as a conservative estimate, we saw hysteresis emerge for high  
439 flow events which exceeded water levels in excess of 1.30 m whilst the actual bedload mobilisation threshold  
440 varied between 0.85 m-1.00 m. We also see a levelling off of the PSD for water levels above 1.40 m which we  
441 interpret to be most likely caused by the presence of a sheet flow of granular material, which would make  
442 it difficult to increase the frequency and magnitude of collisions with the bed (Palucis et al., 2018), thus  
443 reducing the seismic power measured in the high frequencies with increasing water level. We believe that  
444 although there will be a limit on the grain-to-bed interactions during granular sheet flow, there will likely  
445 be increased grain-to-grain interaction which is possible to record with the hydroacoustics. Further analysis  
446 into the frequency characteristics of hydroacoustic data would potentially shed some light on this. However,

447 under this scenario, due to the reduced grain-to-bed interactions, measurable with geophones, studies which  
448 attempt a mass balance based on hysteresis are likely to underestimate the total bedload transported (e.g.  
449 Chao et al., 2015) and the construction of a mass balance using geophones alone will struggle at high flow  
450 rates; a proper analysis of bedload flux will need to consider such non-linearity.

451 In conjunction with the expected hysteresis at high frequencies, previous studies have suggested that  
452 analysing the low frequency band ( $< \sim 1-30$  Hz, e.g. Dietze et al., 2019a; Chao et al., 2015; Burtin et al.,  
453 2008) can effectively isolate the turbulence signal. By focusing on this frequency range, it was believed that  
454 hysteresis would not be observed in the water-level versus PSD plot (Tsai et al., 2012). However, findings  
455 from this study challenge these assumptions, especially in relation to the largest event analysed. Contrary to  
456 expectations, hysteresis is also observed in the lower frequency range, as shown in Supplemental Material S4.  
457 This adds complexity to distinguishing between turbulence and bedload seismic signals, potentially leading  
458 to inaccurate estimations of bedload transport fluxes. However, this analysis may be complicated by the  
459 fact that bedload and turbulence can occupy overlapping frequency ranges, and therefore discrimination of  
460 the frequency bands of interest is very important to avoid contamination of the data. Findings by Turowski  
461 et al. (2013) and Roth et al. (2017), also suggest that water turbulence can in some cases be the dominant  
462 source of seismic noise with the energy transmitted to geophones by bedload being much smaller than the  
463 energy of the water. Therefore, hysteresis that is observed may in fact be related to the changing discharge  
464 rather than the occurrence of bedload transport.

465 Looking forwards, long-term monitoring on this reach will allow us to observe a series of successive events  
466 with varying durations. This will provide us with a more comprehensive understanding of the factors influ-  
467 encing the threshold for bedload mobilisation. In particular, we can assess whether the bedload mobilisation  
468 threshold is primarily influenced by the magnitude of high flow events, the duration of individual events  
469 or the periods between events. Furthermore, we can explore the relationship between these dynamics, the  
470 arrangement of the riverbed structure, and the calculation of the entrainment threshold parameter, Shields  
471 stress.

## 472 5 Conclusions

473 Developing a clear, robust methodology for understanding and digitally monitoring bedload transport and  
474 fluxes is fundamental for informing engineering and flood risk models, particularly with the concerns regard-  
475 ing the increased extreme event occurrence as a result of climate change. The use of seismic sensors is a key  
476 step forward and provides the opportunity to monitor bedload transport in previously inaccessible condi-  
477 tions, however it is clear that care has to be taken when developing the methodological design. Combining  
478 seismic data with other measurement techniques such as hydroacoustic data, as done in this study, allows the

479 independent interpretation of the mobilisation of bedload which can inform a more accurate analysis of the  
480 seismic signal from bedload transport. By studying three successive high flow events, we test for variations in  
481 the flow conditions in an alluvial river that characterise the onset and termination of particle entrainment,  
482 thereby exploring the presence of hysteresis in seismic data as a fingerprint of coarse bedload transport.  
483 Through the use of hydroacoustic data to independently characterise bedload transport, our study found  
484 that bedload transport occurred during all three events but that mobilisation initiated and terminated at  
485 different water levels. Notably, these entrainment thresholds were influenced by preceding events, with a  
486 discernible drop of approximately 15 - 20 % following the largest of the three events. Our study also reveals  
487 that while hysteresis in seismic data, in relation to water level, can sometimes be indicative of bedload trans-  
488 port, it is not a definitive requirement. These findings emphasise the need to enhance our understanding of  
489 the factors that influence the occurrence of bedload transport, particularly in climate change-affected rivers.  
490 Being able to accurately distinguish between distinct seismic signals associated with bedload transport and  
491 water turbulence is crucial, and will enable us to improve our ability to estimate bedload transport fluxes  
492 and gain deeper insights into the complex dynamics of alluvial rivers impacted by climate change. Our study  
493 shows the value in combining seismic and hydroacoustic data for long-term digital monitoring of bedload  
494 transport and suggests the possibility that this combination of data will allow us to identify different gran-  
495 ular flow regimes in the field. Routine monitoring with such digital systems enables us to understand the  
496 systematic evolution in the onset of bedload transport and will be of direct use in calibrating widely used  
497 flood and bedload transport engineering models.

## References

- An, C., Parker, G., Hassan, M., and Fu, X. “Can magic sand cause massive degradation of a gravel-bed river at the decadal scale? Shi-ting River, China”. In: *Geomorphology* 327 (Oct. 2018). DOI: 10.1016/j.geomorph.2018.10.026.
- Bakker, M., Gimbert, F., Geay, T., Misset, C., Zanker, S., and Recking, A. “Field Application and Validation of a Seismic Bedload Transport Model”. en. In: *Journal of Geophysical Research* (2020), p. 22.
- Ballance, L. T., Pitman, R. L., Barlow, J., Pusser, T., D.A., Annamaria I., Hayslip, C., Irvine, L., Steel, D., Baker, C. S., Gillies, D., Baumann-Pickering, S., Trickey, J. S., and Gisborne, B. “Acoustic recordings, biological observations, and genetic identification of a rare(?) beaked whale in the North Pacific: *Mesoplodon carlhubbsi*”. en. In: *Marine Mammal Science* (2023). eprint: <https://onlinelibrary.wiley.com/doi/pdf/10.1111/mms.13059>. ISSN: 1748-7692. DOI: 10.1111/mms.13059. URL: <https://onlinelibrary.wiley.com/doi/abs/10.1111/mms.13059> (visited on 10/30/2023).
- Barker, L., Hannaford, J., Muchan, K., Turner, S., and Parry, S. “The winter 2015/2016 floods in the UK: a hydrological appraisal”. en. In: *Weather* 71.12 (2016), pp. 324–333. ISSN: 1477-8696. DOI: 10.1002/wea.2822. URL: <https://onlinelibrary.wiley.com/doi/abs/10.1002/wea.2822> (visited on 10/20/2023).
- Barrière, J., Oth, A., Hostache, R., and Krein, A. “Bed load transport monitoring using seismic observations in a low-gradient rural gravel bed stream: Seismic monitoring of bedload transport”. en. In: *Geophysical Research Letters* 42.7 (Apr. 2015), pp. 2294–2301. ISSN: 00948276. DOI: 10.1002/2015GL063630. URL: <http://doi.wiley.com/10.1002/2015GL063630> (visited on 10/28/2020).
- Belleudy, P., Valette, A., and Graff, B. “Monitoring of bedload in river beds with an hydrophone: first trials of signal analyses”. en. In: *Dittrich, A.; Koll, K.; Aberle, J.; Geisenhainer, P. (Hg.): River Flow 2010* (2010). URL: <https://hdl.handle.net/20.500.11970/99836>.
- Bogen, J. “The hysteresis effect of sediment transport systems”. en. In: *Norsk Geografisk Tidsskrift - Norwegian Journal of Geography* 34.1 (Jan. 1980), pp. 45–54. ISSN: 0029-1951, 1502-5292. DOI:

526 10.1080/00291958008545338. URL: <http://www.tandfonline.com/doi/abs/10.1080/>  
527 00291958008545338 (visited on 11/16/2020).

528 Bountourakis, V., Elvander, F., and Pulkki, V. *Using optimal mass transport in bearing-time*  
529 *records for underwater target localization and tracking*. June 2023.

530 Brasington, J., Langham, J., and Rumsby, B. “Methodological sensitivity of morphometric esti-  
531 mates of coarse fluvial sediment transport”. en. In: *Geomorphology* 53.3 (July 2003), pp. 299–316.  
532 ISSN: 0169-555X. DOI: 10.1016/S0169-555X(02)00320-3. URL: [https://www.sciencedirect.](https://www.sciencedirect.com/science/article/pii/S0169555X02003203)  
533 [com/science/article/pii/S0169555X02003203](https://www.sciencedirect.com/science/article/pii/S0169555X02003203) (visited on 02/01/2023).

534 Brasington, J., Rumsby, B. T., and Mcvey, R. A. “Monitoring and modelling morphological  
535 change in a braided gravel-bed river using high resolution GPS-based survey”. en. In: (2000),  
536 p. 18.

537 Bunte, K. and Abt, S. R. “Effect of sampling time on measured gravel bed load transport rates  
538 in a coarse-bedded stream”. In: *Water Resources Research* 41.11 (2005). DOI: [https://doi.org/](https://doi.org/10.1029/2004WR003880)  
539 [10.1029/2004WR003880](https://doi.org/10.1029/2004WR003880). URL: [https://agupubs.onlinelibrary.wiley.com/doi/10.1029/](https://agupubs.onlinelibrary.wiley.com/doi/10.1029/2004wr003880)  
540 [2004wr003880](https://agupubs.onlinelibrary.wiley.com/doi/10.1029/2004wr003880) (visited on 10/30/2023).

541 Bunte, K., Abt, S.R., Potyondy, J. P., and Ryan, S. E. “Measurement of Coarse Gravel and  
542 Cobble Transport Using Portable Bedload Traps”. EN. In: *Journal of Hydraulic Engineering*  
543 130.9 (Sept. 2004). Publisher: American Society of Civil Engineers, pp. 879–893. ISSN: 0733-  
544 9429. DOI: 10.1061/(ASCE)0733-9429(2004)130:9(879). URL: [https://ascelibrary.org/](https://ascelibrary.org/doi/10.1061/%28ASCE%290733-9429%282004%29130%3A9%28879%29)  
545 [doi/10.1061/%28ASCE%290733-9429%282004%29130%3A9%28879%29](https://ascelibrary.org/doi/10.1061/%28ASCE%290733-9429%282004%29130%3A9%28879%29) (visited on 10/30/2023).

546 Burtin, A., Bollinger, L., Vergne, J., Cattin, R., and Nábělek, J. L. “Spectral analysis of seismic  
547 noise induced by rivers: A new tool to monitor spatiotemporal changes in stream hydrodynamics”.  
548 en. In: *Journal of Geophysical Research* 113.B5 (May 2008). ISSN: 0148-0227. DOI: 10.1029/  
549 2007JB005034. URL: <http://doi.wiley.com/10.1029/2007JB005034> (visited on 10/28/2020).

550 Burtin, A., Hovius, N., McArdell, B. W., Turowski, J. M., and Vergne, J. “Seismic constraints  
551 on dynamic links between geomorphic processes and routing of sediment in a steep mountain  
552 catchment”. en. In: *Earth Surface Dynamics* 2.1 (Jan. 2014), pp. 21–33. ISSN: 2196-632X. DOI:

553 10.5194/esurf-2-21-2014. URL: <https://esurf.copernicus.org/articles/2/21/2014/>  
554 (visited on 10/28/2020).

555 Burtin, A., Vergne, J., Rivera, L., and Dubernet, P. “Location of river-induced seismic signal  
556 from noise correlation functions: Location of river seismic signal”. en. In: *Geophysical Journal*  
557 *International* 182.3 (Sept. 2010), pp. 1161–1173. ISSN: 0956540X. DOI: 10.1111/j.1365-246X.  
558 2010.04701.x. URL: [https://academic.oup.com/gji/article-lookup/doi/10.1111/j.  
559 1365-246X.2010.04701.x](https://academic.oup.com/gji/article-lookup/doi/10.1111/j.1365-246X.2010.04701.x) (visited on 10/28/2020).

560 Chao, W.-A., Wu, Y.-M., Zhao, L., Tsai, V. C., and Chen, C.-H. “Seismologically determined  
561 bedload flux during the typhoon season”. en. In: *Scientific Reports* 5.1 (July 2015), p. 8261. ISSN:  
562 2045-2322. DOI: 10.1038/srep08261. URL: <http://www.nature.com/articles/srep08261>  
563 (visited on 10/28/2020).

564 Chelmiecki, W. and Krzemień, K. “Channel Typology for the River Feshie in the Cairngorm Mts,  
565 Scotland”. en. In: *Prace Geograficzne* (1999), p. 12.

566 Church, M. “Bed Material Transport and the Morphology of Alluvial River Channels”. In: *Annual*  
567 *Review of Earth and Planetary Sciences* 34.1 (2006), pp. 325–354. DOI: 10.1146/annurev.earth.  
568 33.092203.122721. URL: [https://doi.org/10.1146/annurev.earth.  
569 33.092203.122721](https://doi.org/10.1146/annurev.earth.33.092203.122721) (visited on 04/12/2021).

570 Church, M., Hassan, M. A., and Wolcott, J. F. “Stabilizing self-organized structures in gravel-  
571 bed stream channels: Field and experimental observations”. en. In: *Water Resources Research*  
572 34.11 (1998). eprint: <https://onlinelibrary.wiley.com/doi/pdf/10.1029/98WR00484>, pp. 3169–  
573 3179. ISSN: 1944-7973. DOI: 10.1029/98WR00484. URL: [https://onlinelibrary.wiley.com/  
574 doi/abs/10.1029/98WR00484](https://onlinelibrary.wiley.com/doi/abs/10.1029/98WR00484) (visited on 03/10/2023).

575 Cox, J. R., Huismans, Y., Knaake, S. M., Leuven, J. R. F. W., Vellinga, N. E., Vegt, M. van der,  
576 Hoitink, A. J. F., and Kleinhans, M. G. “Anthropogenic Effects on the Contemporary Sediment  
577 Budget of the Lower Rhine-Meuse Delta Channel Network”. en. In: *Earth’s Future* 9.7 (2021).  
578 eprint: <https://onlinelibrary.wiley.com/doi/pdf/10.1029/2020EF001869>, e2020EF001869. ISSN:  
579 2328-4277. DOI: 10.1029/2020EF001869. URL: [https://onlinelibrary.wiley.com/doi/abs/  
580 10.1029/2020EF001869](https://onlinelibrary.wiley.com/doi/abs/10.1029/2020EF001869) (visited on 10/30/2023).



581 Dean, Tim. “The seismic signature of rain”. en. In: *ASEG Extended Abstracts* 2018.1 (Dec. 2018),  
582 pp. 1–8. ISSN: 2202-0586. DOI: 10.1071/ASEG2018abP068. URL: <https://www.tandfonline.com/doi/full/10.1071/ASEG2018abP068> (visited on 12/06/2022).

584 Dey, S. *Fluvial Hydrodynamics*. en. GeoPlanet: Earth and Planetary Sciences. Berlin, Heidelberg:  
585 Springer Berlin Heidelberg, 2014. ISBN: 978-3-642-19061-2 978-3-642-19062-9. DOI: 10.1007/978-  
586 3-642-19062-9. URL: <http://link.springer.com/10.1007/978-3-642-19062-9> (visited on  
587 11/20/2020).

588 Dietze, M. and Gimbert, F. “The seismic view on sediment laden ephemeral flows – modelling of  
589 ground motion data for fluid and bedload dynamics in the Arroyo de los Piños”. en. In: (2019),  
590 p. 10.

591 Dietze, M., Lagarde, S., Halfi, E., Laronne, J. B., and Turowski, J. M. “Joint Sensing of Bedload  
592 Flux and Water Depth by Seismic Data Inversion”. en. In: *Water Resources Research* 55.11  
593 (2019), pp. 9892–9904. ISSN: 1944-7973. DOI: <https://doi.org/10.1029/2019WR026072>. URL:  
594 <https://agupubs.onlinelibrary.wiley.com/doi/abs/10.1029/2019WR026072> (visited on  
595 02/26/2021).

596 Downs, P. W., Soar, P. J., and Taylor, A. “The anatomy of effective discharge: the dynamics  
597 of coarse sediment transport revealed using continuous bedload monitoring in a gravel-bed river  
598 during a very wet year: Dynamics of coarse sediment transport using continuous monitoring”. en.  
599 In: *Earth Surface Processes and Landforms* 41.2 (Feb. 2016), pp. 147–161. ISSN: 01979337. DOI:  
600 10.1002/esp.3785. URL: <http://doi.wiley.com/10.1002/esp.3785> (visited on 10/28/2020).

601 Ferguson, R. I. and Werritty, A. “Bar Development and Channel Changes in the Gravelly River  
602 Feshie, Scotland”. en. In: *Modern and Ancient Fluvial Systems*. Ed. by J. D. Collinson and J.  
603 Lewin. Oxford, UK: Blackwell Publishing Ltd., Feb. 1983, pp. 181–193. ISBN: 978-1-4443-0377-3  
604 978-0-632-00997-8. DOI: 10.1002/9781444303773.ch14. URL: <http://doi.wiley.com/10.1002/9781444303773.ch14> (visited on 10/28/2020).

605  
606 Gaeuman, D. “Mechanics of Bedload Rating Curve Shifts and Bedload Hysteresis in the Trinity  
607 River, California”. en. In: (2010).

608 Geay, T., Zanker, S., Misset, C., and Recking, A. “Passive Acoustic Measurement of Bedload  
609 Transport: Toward a Global Calibration Curve?” en. In: *Journal of Geophysical Research: Earth*  
610 *Surface* 125.8 (2020). \_eprint: <https://onlinelibrary.wiley.com/doi/pdf/10.1029/2019JF005242>,  
611 e2019JF005242. ISSN: 2169-9011. DOI: 10.1029/2019JF005242. URL: <https://onlinelibrary.wiley.com/doi/abs/10.1029/2019JF005242> (visited on 01/13/2022).

613 Gimbert, F., Tsai, V. C., and Lamb, M. P. “A physical model for seismic noise generation by  
614 turbulent flow in rivers”. en. In: *Journal of Geophysical Research: Earth Surface* 119.10 (Oct.  
615 2014), pp. 2209–2238. ISSN: 21699003. DOI: 10.1002/2014JF003201. URL: <http://doi.wiley.com/10.1002/2014JF003201> (visited on 10/28/2020).

617 Gomez, B. and Soar, P. J. “Bedload transport: beyond intractability”. In: *Royal Society Open*  
618 *Science* 9.3 (Mar. 2022). Publisher: Royal Society, p. 211932. DOI: 10.1098/rsos.211932. URL:  
619 <https://royalsocietypublishing.org/doi/10.1098/rsos.211932> (visited on 10/30/2023).

620 Hassan, M. A., Egozi, R., and Parker, G. “Experiments on the effect of hydrograph characteristics  
621 on vertical grain sorting in gravel bed rivers”. en. In: *Water Resources Research* 42.9 (2006).  
622 ISSN: 1944-7973. DOI: <https://doi.org/10.1029/2005WR004707>. URL: <https://agupubs.onlinelibrary.wiley.com/doi/abs/10.1029/2005WR004707> (visited on 12/03/2020).

624 Hsu, L., Finnegan, N. J., and Brodsky, E. E. “A seismic signature of river bedload transport  
625 during storm events”. en. In: *Geophysical Research Letters* 38.13 (July 2011). ISSN: 00948276.  
626 DOI: 10.1029/2011GL047759. URL: <http://doi.wiley.com/10.1029/2011GL047759> (visited  
627 on 10/28/2020).

628 Jain, R., Tschisgale, S., and Fröhlich, J. “Impact of shape: DNS of sediment transport with non-  
629 spherical particles”. en. In: *Journal of Fluid Mechanics* 916 (June 2021). Publisher: Cambridge  
630 University Press, A38. ISSN: 0022-1120, 1469-7645. DOI: 10.1017/jfm.2021.214. URL: <https://www.cambridge.org/core/journals/journal-of-fluid-mechanics/article/impact-of-shape-dns-of-sediment-transport-with-nonspherical-particles/0B3ED0C2B19C84AB97EB83F7362389A8> (visited on 05/31/2023).

634 Kothyari, U. C. and Jain, R. K. “Influence of cohesion on the incipient motion condition of  
635 sediment mixtures”. en. In: *Water Resources Research* 44.4 (2008). ISSN: 1944-7973. DOI: 10.

636 1029/2007WR006326. URL: <https://onlinelibrary.wiley.com/doi/abs/10.1029/2007WR>  
637 006326 (visited on 03/10/2023).

638 Kuhnle, R. A. “Bed load transport during rising and falling stages on two small streams”. en. In:  
639 *Earth Surface Processes and Landforms* 17.2 (1992), pp. 191–197. ISSN: 1096-9837. DOI: <https://doi.org/10.1002/esp.3290170206>. URL: [https://onlinelibrary.wiley.com/doi/abs/](https://onlinelibrary.wiley.com/doi/abs/10.1002/esp.3290170206)  
640 [10.1002/esp.3290170206](https://onlinelibrary.wiley.com/doi/abs/10.1002/esp.3290170206). URL: [https://onlinelibrary.wiley.com/doi/abs/](https://onlinelibrary.wiley.com/doi/abs/10.1002/esp.3290170206)  
641 [10.1002/esp.3290170206](https://onlinelibrary.wiley.com/doi/abs/10.1002/esp.3290170206) (visited on 12/03/2020).

642 Lagarde, S., Dietze, M., Gimbert, F., Laronne, J. B., Turowski, J. M., and Halfi, E. “Grain-  
643 Size Distribution and Propagation Effects on Seismic Signals Generated by Bedload Transport”.  
644 en. In: *Water Resources Research* 57.4 (2021). ISSN: 1944-7973. DOI: [https://doi.org/10.](https://doi.org/10.1029/2020WR028700)  
645 [1029/2020WR028700](https://doi.org/10.1029/2020WR028700). URL: [https://agupubs.onlinelibrary.wiley.com/doi/abs/10.1029/](https://agupubs.onlinelibrary.wiley.com/doi/abs/10.1029/2020WR028700)  
646 [2020WR028700](https://agupubs.onlinelibrary.wiley.com/doi/abs/10.1029/2020WR028700) (visited on 05/31/2021).

647 Lee, K. T., Liu, Yi-Liang, and Cheng, Kai-Hung. “Experimental investigation of bedload trans-  
648 port processes under unsteady flow conditions”. en. In: *Hydrological Processes* 18.13 (2004),  
649 pp. 2439–2454. ISSN: 1099-1085. DOI: <https://doi.org/10.1002/hyp.1473>. URL: <https://onlinelibrary.wiley.com/doi/abs/10.1002/hyp.1473>. URL: <https://onlinelibrary.wiley.com/doi/abs/10.1002/hyp.1473> (visited on 12/03/2020).

650

651 Lisle, T. E. and Madej, M. A. “Spatial variation in armouring in a channel with high sediment  
652 supply”. en. In: *Dynamics of gravel-bed rivers* (1992), pp. 277–293.

653

654 Luo, M., Jiang, Y., Wang, S., Liu, X., and Huang, E. “The effect of stress history on fluctuation of  
655 bedload transport rate and bed topography in gravel-bed streams”. en. In: *Journal of Hydrology*  
656 616 (Jan. 2023), p. 128732. ISSN: 00221694. DOI: 10.1016/j.jhydro.2022.128732. URL: <https://linkinghub.elsevier.com/retrieve/pii/S0022169422013026> (visited on 06/01/2023).

657

658 Mao, L. “The effect of hydrographs on bed load transport and bed sediment spatial arrangement”.  
659 en. In: *Journal of Geophysical Research: Earth Surface* 117.F3 (2012). ISSN: 2156-2202. DOI:  
660 <https://doi.org/10.1029/2012JF002428>. URL: [https://agupubs.onlinelibrary.wiley.](https://agupubs.onlinelibrary.wiley.com/doi/abs/10.1029/2012JF002428)  
[com/doi/abs/10.1029/2012JF002428](https://agupubs.onlinelibrary.wiley.com/doi/abs/10.1029/2012JF002428) (visited on 11/30/2020).

661

662 Mao, L., Dell’Agnese, A., Huincache, C., Penna, D., Engel, M., Niedrist, G., and Comiti, F.  
663 “Bedload hysteresis in a glacier-fed mountain river”. en. In: *Earth Surface Processes and Land-*  
*forms* 39.7 (2014). eprint: <https://onlinelibrary.wiley.com/doi/pdf/10.1002/esp.3563>, pp. 964–

664 976. ISSN: 1096-9837. DOI: <https://doi.org/10.1002/esp.3563>. URL: <https://onlinelibrary.wiley.com/doi/abs/10.1002/esp.3563> (visited on 11/30/2020).

666 Ockelford, A., Woodcock, S., and Haynes, H. “The impact of inter-flood duration on non-cohesive  
667 sediment bed stability”. en. In: *Earth Surface Processes and Landforms* 44.14 (2019). eprint:  
668 <https://onlinelibrary.wiley.com/doi/pdf/10.1002/esp.4713>, pp. 2861–2871. ISSN: 1096-9837. DOI:  
669 10.1002/esp.4713. URL: <https://onlinelibrary.wiley.com/doi/abs/10.1002/esp.4713>  
670 (visited on 03/06/2023).

671 Palucis, M. C., Ulizio, T., Fuller, B., and Lamb, M. P. “Intense Granular Sheetflow in Steep  
672 Streams”. en. In: *Geophysical Research Letters* 45.11 (2018), pp. 5509–5517. ISSN: 1944-8007.  
673 DOI: 10.1029/2018GL077526. URL: [https://onlinelibrary.wiley.com/doi/abs/10.1029/  
674 2018GL077526](https://onlinelibrary.wiley.com/doi/abs/10.1029/2018GL077526) (visited on 10/30/2023).

675 Pitlick, J., Cui, Y., and Wilcock, P. “Manual for Computing Bed Load Transport Using BAGS  
676 (Bedload Assessment for Gravel-bed Streams) Software”. In: (Jan. 2009).

677 Reid, I., Frostick, L. E., and Layman, J. T. “The incidence and nature of bedload transport during  
678 flood flows in coarse-grained alluvial channels”. en. In: *Earth Surface Processes and Landforms*  
679 10.1 (1985), pp. 33–44. ISSN: 1096-9837. DOI: 10.1002/esp.3290100107. URL: [https://online  
680 library.wiley.com/doi/abs/10.1002/esp.3290100107](https://onlinelibrary.wiley.com/doi/abs/10.1002/esp.3290100107) (visited on 09/14/2021).

681 Rickenmann, D. “Hyperconcentrated Flow and Sediment Transport at Steep Slopes”. EN. In:  
682 *Journal of Hydraulic Engineering* 117.11 (Nov. 1991). Publisher: American Society of Civil En-  
683 gineers, pp. 1419–1439. ISSN: 0733-9429. DOI: 10.1061/(ASCE)0733-9429(1991)117:11(1419).  
684 URL: [https://ascelibrary.org/doi/10.1061/%28ASCE%290733-9429%281991%29117%3A11%  
685 281419%29](https://ascelibrary.org/doi/10.1061/%28ASCE%290733-9429%281991%29117%3A11%281419%29) (visited on 10/30/2023).

686 Rindraharisaona, E. J., Réchou, A., Fontaine, F. R., Barruol, G., Stamenoff, P., Boudevillain,  
687 B., Rigaud-Louise, F., and Delcher, E. “Seismic Signature of Rain and Wind Inferred From  
688 Seismic Data”. en. In: *Earth and Space Science* 9.10 (2022). ISSN: 2333-5084. DOI: 10.1029/  
689 2022EA002328. URL: <https://onlinelibrary.wiley.com/doi/abs/10.1029/2022EA002328>  
690 (visited on 12/06/2022).

691 Roth, D. L., Brodsky, E.E., Finnegan, N.J., Rickenmann, D., Turowski, J.M., and Badoux, A.  
692 “Bed load sediment transport inferred from seismic signals near a river”. en. In: *Journal of*  
693 *Geophysical Research: Earth Surface* 121.4 (Apr. 2016), pp. 725–747. ISSN: 2169-9003, 2169-9011.  
694 DOI: 10.1002/2015JF003782. URL: [https://onlinelibrary.wiley.com/doi/abs/10.1002/](https://onlinelibrary.wiley.com/doi/abs/10.1002/2015JF003782)  
695 [2015JF003782](https://onlinelibrary.wiley.com/doi/abs/10.1002/2015JF003782) (visited on 10/28/2020).

696 Roth, D. L., Finnegan, N. J., Brodsky, E. E., Rickenmann, D., Turowski, J. M., Badoux, A.,  
697 and Gimbert, F. “Bed load transport and boundary roughness changes as competing causes  
698 of hysteresis in the relationship between river discharge and seismic amplitude recorded near  
699 a steep mountain stream”. en. In: *Journal of Geophysical Research: Earth Surface* 122.5 (May  
700 2017), pp. 1182–1200. ISSN: 21699003. DOI: 10.1002/2016JF004062. URL: [http://doi.wiley.](http://doi.wiley.com/10.1002/2016JF004062)  
701 [com/10.1002/2016JF004062](http://doi.wiley.com/10.1002/2016JF004062) (visited on 11/16/2020).

702 Schmandt, B., Aster, R. C., Scherler, D., Tsai, V. C., and Karlstrom, K. “Multiple fluvial pro-  
703 cesses detected by riverside seismic and infrasound monitoring of a controlled flood in the Grand  
704 Canyon”. en. In: *Geophysical Research Letters* 40.18 (Sept. 2013), pp. 4858–4863. ISSN: 0094-  
705 8276, 1944-8007. DOI: 10.1002/grl.50953. URL: [https://onlinelibrary.wiley.com/doi/](https://onlinelibrary.wiley.com/doi/abs/10.1002/grl.50953)  
706 [abs/10.1002/grl.50953](https://onlinelibrary.wiley.com/doi/abs/10.1002/grl.50953) (visited on 10/28/2020).

707 Thorne, P. D. “An overview of underwater sound generated by interparticle collisions and its  
708 application to the measurements of coarse sediment bedload transport”. en. In: *Earth Surface*  
709 *Dynamics* 2.2 (Dec. 2014), pp. 531–543. ISSN: 2196-632X. DOI: 10.5194/esurf-2-531-2014.  
710 URL: <https://esurf.copernicus.org/articles/2/531/2014/> (visited on 10/28/2020).

711 Tsai, V. C., Minchew, B., Lamb, M. P., and Ampuero, J.-P. “A physical model for seismic noise  
712 generation from sediment transport in rivers”. en. In: *Geophysical Research Letters* 39.2 (Jan.  
713 2012). ISSN: 00948276. DOI: 10.1029/2011GL050255. URL: [http://doi.wiley.com/10.1029/](http://doi.wiley.com/10.1029/2011GL050255)  
714 [2011GL050255](http://doi.wiley.com/10.1029/2011GL050255) (visited on 10/28/2020).

715 Turowski, J. M., Badoux, A., and Rickenmann, D. “Start and end of bedload transport in  
716 gravel-bed streams”. en. In: *Geophysical Research Letters* 38.4 (Feb. 2011). ISSN: 00948276. DOI:  
717 10.1029/2010GL046558. URL: <http://doi.wiley.com/10.1029/2010GL046558> (visited on  
718 10/28/2020).

719 Turowski, J. M., Böckli, M., Rickenmann, D., and Beer, A. R. “Field measurements of the energy  
720 delivered to the channel bed by moving bed load and links to bedrock erosion”. en. In: *Journal*  
721 *of Geophysical Research: Earth Surface* 118.4 (Dec. 2013), pp. 2438–2450. ISSN: 21699003. DOI:  
722 10.1002/2013JF002765. URL: <http://doi.wiley.com/10.1002/2013JF002765> (visited on  
723 10/28/2020).

724 Turowski, J. M., Wyss, C. R., and Beer, A. R. “Grain size effects on energy delivery to the  
725 streambed and links to bedrock erosion”. en. In: *Geophysical Research Letters* 42.6 (Mar. 2015),  
726 pp. 1775–1780. ISSN: 0094-8276, 1944-8007. DOI: 10.1002/2015GL063159. URL: <https://onlinelibrary.wiley.com/doi/abs/10.1002/2015GL063159> (visited on 10/28/2020).

728 Vore, M. E., Bartholomaus, T. C., Winberry, J. P., Walter, J. I., and Amundson, J. M. “Seismic  
729 Tremor Reveals Spatial Organization and Temporal Changes of Subglacial Water System”. en.  
730 In: *Journal of Geophysical Research: Earth Surface* 124.2 (2019), pp. 427–446. ISSN: 2169-9011.  
731 DOI: 10.1029/2018JF004819. URL: [https://onlinelibrary.wiley.com/doi/abs/10.1029/](https://onlinelibrary.wiley.com/doi/abs/10.1029/2018JF004819)  
732 [2018JF004819](https://onlinelibrary.wiley.com/doi/abs/10.1029/2018JF004819) (visited on 01/23/2023).

733 Welch, P. “The use of fast Fourier transform for the estimation of power spectra: A method  
734 based on time averaging over short, modified periodograms”. In: *IEEE Transactions on Au-*  
735 *dio and Electroacoustics* 15.2 (June 1967). Conference Name: IEEE Transactions on Audio and  
736 Electroacoustics, pp. 70–73. ISSN: 1558-2582. DOI: 10.1109/TAU.1967.1161901. URL: <https://ieeexplore.ieee.org/document/1161901> (visited on 11/10/2023).

738 Wilcock, P. R. and Crowe, J. C. “Surface-based Transport Model for Mixed-Size Sediment”. en.  
739 In: *Journal of Hydraulic Engineering* 129.2 (Feb. 2003), pp. 120–128. ISSN: 0733-9429, 1943-7900.  
740 DOI: 10.1061/(ASCE)0733-9429(2003)129:2(120). URL: [http://ascelibrary.org/doi/10.](http://ascelibrary.org/doi/10.1061/%28ASCE%290733-9429%282003%29129%3A2%28120%29)  
741 [1061/%28ASCE%290733-9429%282003%29129%3A2%28120%29](http://ascelibrary.org/doi/10.1061/%28ASCE%290733-9429%282003%29129%3A2%28120%29) (visited on 07/01/2021).

742 Wilcock, W. S. D., Webb, S. C., and Bjarnason, I. Th. “The effect of local wind on seismic  
743 noise near 1 Hz at the MELT site and in iceland”. In: *Bulletin of the Seismological Society of*  
744 *America* 89.6 (Dec. 1999), pp. 1543–1557. ISSN: 0037-1106. DOI: 10.1785/BSSA0890061543. URL:  
745 <https://doi.org/10.1785/BSSA0890061543> (visited on 03/20/2023).

746 Wolman, M. G. “A method of sampling coarse river-bed material”. en. In: *Eos, Transactions*  
747 *American Geophysical Union* 35.6 (1954), pp. 951–956. ISSN: 2324-9250. DOI: 10.1029/TR035i

748 006p00951. URL: <https://onlinelibrary.wiley.com/doi/abs/10.1029/TR035i006p00951>

749 (visited on 10/20/2023).

**Audio 1:** Hydrophone audio recording from 13:30 on the 30th September 2023 during the water level peak of the September-October event showing the lower frequency signals observed in the hydroacoustic data, attributed to larger grains being transported.

**Audio 2:** Hydrophone audio recording from 17:15 on the 30th September 2023 showing the higher frequency signals recorded at water levels below approximately 1.6 m during the September-October event which were categorised as the movement of smaller particles.

**Audio 3:** Hydrophone audio recording from 21:45 on the 30th September 2023 during of the background turbulence signal following the cessation of bedload transport during the September-October event.